The Chandra Deep Field-North Survey and the Cosmic X-ray Background

By W. Nielsen Brandt, David M. Alexander, Franz E. Bauer, & Ann E. Hornschemeier (for the Chandra Deep Field-North team)

Department of Astronomy & Astrophysics, 525 Davey Laboratory, The Pennsylvania State University, University Park, PA 16802, USA

Chandra has performed a 1.4 Ms survey centred on the Hubble Deep Field-North (HDF-N), probing the X-ray Universe 55–550 times deeper than was possible with pre-*Chandra* missions. We describe the detected point and extended X-ray sources and discuss their overall multiwavelength (optical, infrared, submillimeter, and radio) properties. Special attention is paid to the HDF-N X-ray sources, luminous infrared starburst galaxies, optically faint X-ray sources, and high-to-extreme redshift AGN. We also describe how stacking analyses have been used to probe the average X-ray emission properties of normal and starburst galaxies at cosmologically interesting distances. Finally, we discuss plans to extend the survey and argue that a 5–10 Ms *Chandra* survey would lay key groundwork for future missions such as *XEUS* and *Generation-X*.

Keywords: diffuse radiation; surveys; cosmology: observations; galaxies: active; X-rays: galaxies; X-rays: general

1. Introduction

(*a*) *The Cosmic X-ray Background*

The cosmic X-ray background was the first cosmic background radiation discovered (Giacconi *et al.* 1962) and has $\approx$ 10% of the energy density of the cosmic microwave background (see, e.g., Fabian & Barcons 1992 and Hasinger 2000 for reviews). In contrast to the cosmic microwave background, the cosmic X-ray background is comprised of the integrated contributions from a large number of discrete sources. The X-ray background thus represents the summed emission from all X-ray sources since the Universe was less than a billion years old, and by surveying it we can learn about the nature and evolution of X-ray emitting objects over most of the history of the Universe.

The X-ray background is detected over a broad energy band from $\approx$ 0.1–200 keV, peaking in energy density from 20–40 keV; the logarithmic frequency/energy coverage is comparable to that of the far-infrared to extreme ultraviolet bandpass. Current deep imaging surveys of the X-ray background, however, have been primarily conducted in the narrower $\approx$ 0.1–12 keV band due largely to technological limitations.

Observations with the new generation of X-ray observatories, *Chandra* (Weisskopf *et al.* 2000) and *XMM-Newton* (Jansen *et al.* 2001), have revolutionised studies of the X-ray background and the sources that comprise it. Early observations with *Chandra* resolved most of the 2–8 keV background into point sources (e.g., Brandt *et al.* 2000; Mushotzky *et al.* 2000; Giacconi *et al.* 2001); most of the 0.5–2 keV background had already been resolved by *ROSAT* (e.g., Hasinger *et al.* 1998). The accurate positions from the new observatories, particularly *Chandra*, also allow X-ray sources to be matched unambiguously to (often faint) multiwavelength counterparts. X-ray surveys have finally reached the depths needed to complement the most sensitive surveys in the radio, submillimeter, infrared, and optical bands. The focus has now shifted from simply resolving the X-ray background to understanding in detail the sources that comprise it at all X-ray fluxes. While it is clear that massive, accreting black holes produce the bulk of the X-ray background, the deepest X-ray surveys are now allowing the study of other source classes, including starburst and normal galaxies.

In this article, we will review some of the current results from the ongoing *Chandra* Deep Field-North (CDF-N) survey. Other ongoing deep X-ray surveys that have published results at present include the *Chandra* Deep Field South Survey (e.g., Giacconi *et al.* 2002; Rosati *et al.* 2002), the Lockman Hole Survey (e.g., Hasinger *et al.* 2001; Lehmann *et al.* 2001), and the SSA13 Survey (e.g., Mushotzky *et al.* 2000; Barger *et al.* 2001a). Many other important X-ray surveys are being performed over larger solid angles to shallower depths.

Throughout this article we adopt $H_0 = 65$ km s^{-1} Mpc^{-1}, $\Omega_{\rm M} = 1/3$, and $\Omega_\Lambda = 2/3$.

(*b*) *The Chandra Deep Field-North Survey*

The CDF-N survey is currently the deepest X-ray survey ever performed. It is comprised of 1.4 Ms (16.2 days) of exposure with the *Chandra* Advanced CCD Imaging Spectrometer (ACIS) covering an $\approx 18' \times 22'$ field (see Fig. 1) centred on the Hubble Deep Field-North (HDF-N; see Ferguson *et al.* 2000); these observations are publicly available. This is an excellent field for study, since it already has intensive coverage at optical, infrared, submillimeter and radio wavelengths (see Ferguson *et al.* 2000 for a review). More than 800 spectroscopic redshifts have been obtained in the field (e.g., Cohen *et al.* 2000). In the soft (0.5–2 keV) and hard (2–8 keV) X-ray bands, the *Chandra* data reach fluxes ≈ 55 and ≈ 550 times fainter than surveys by previous X-ray missions (see Fig. 2). Near the centre of the field, sources with count rates as low as ≈ 1 count per 2 days can be detected. Source densities near the soft-band and hard-band flux limits are ≈ 7200 deg^{-2} and ≈ 4200 deg^{-2} (e.g., Brandt *et al.* 2001b; Cowie *et al.* 2002); the fraction of the X-ray background resolved in the soft and hard bands is $> 90\%$ and $> 80\%$, respectively (the main uncertainty in the resolved fraction is the absolute normalisation of the background itself). Source positions are typically accurate to better than $1''$ over the entire field, allowing multiwavelength counterparts to be identified reliably.

The CDF-N team includes ≈ 20 researchers from The Pennsylvania State University, The University of Hawaii, The University of Wisconsin, The Massachusetts Institute of Technology, The California Institute of Technology, and Carnegie Mellon University. To see all the contributors to the various CDF-N projects, please refer to the author lists of the cited CDF-N publications.

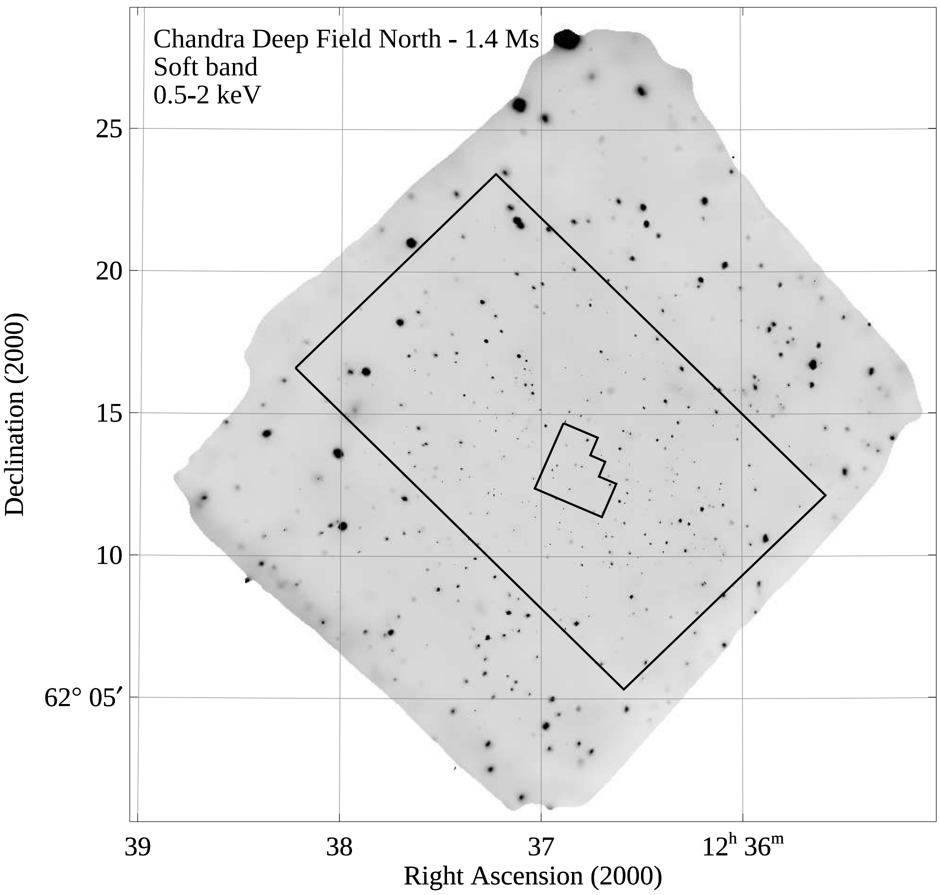

Figure 1. Adaptively smoothed and exposure-map corrected image of the CDF-N in the soft band. The adaptive smoothing has been performed using the code of Ebeling *et al.* (2002) at the 2.5σ level, and the grayscale is linear. Source sizes appear to change across the field due to the spatial dependence of the instrumental point spread function. The small polygon indicates the HDF-N, and the large rectangle indicates the GOODS area (see §3b).

2. Some Key Results from the Survey

(*a*) *Detected Point and Extended Sources*

The CDF-N data have been searched intensively for point sources using the *Chandra* X-ray Center's WAVDETECT algorithm (Freeman *et al.* 2002). At a WAVDETECT false-positive probability threshold of 1×10^{-7}, ≈ 430 independent sources are detected in the 1.4 Ms exposure. In addition, a substantial number of sources have been found at lower significance levels that are spatially correlated with objects found at other wavelengths (e.g., optically bright galaxies). Many of these sources are real, but it is more difficult to define a complete X-ray flux-limited sample of

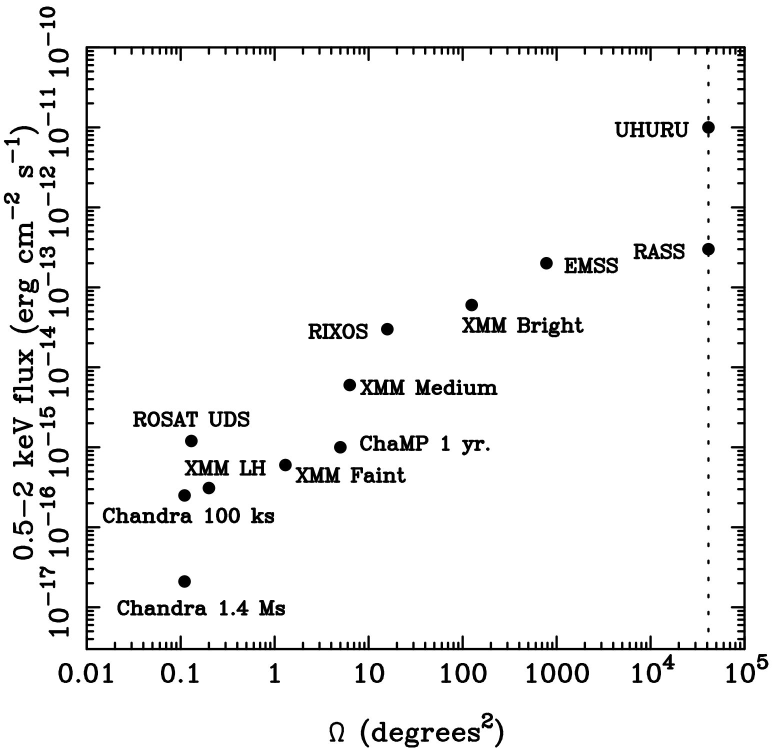

Figure 2. A selection of extragalactic X-ray surveys in the 0.5–2 keV flux limit versus solid angle, Ω, plane. Shown are the *Uhuru* survey, the *ROSAT* All-Sky Survey (RASS), the *Einstein* Extended Medium-Sensitivity Survey (EMSS), the *ROSAT* International X-ray/Optical Survey (RIXOS), the *XMM-Newton* Serendipitious Surveys (*XMM* Bright, *XMM* Medium, *XMM* Faint), the *Chandra* Multiwavelength Project (ChaMP), the *ROSAT* Ultra Deep Survey (*ROSAT* UDS), the deep *XMM-Newton* survey of the Lockman Hole (*XMM* LH), *Chandra* 100 ks surveys, and *Chandra* 1.4 Ms surveys (i.e., the CDF-N). Although each of the surveys shown clearly has a range of flux limits across its solid angle, we have generally shown the most sensitive flux limit. The vertical dot-dashed line shows the solid angle of the whole sky. Adapted from Brandt *et al.* (2001b).

these sources. In the full band (0.5–8 keV), the typical source has ≈ 90 counts which is too small for detailed X-ray spectral analysis. Assessment of spectral hardness is possible, however, and X-ray spectral analysis can be performed for the brighter sources in the field. Catalogs of the detected sources and related analysis products have been made publicly available for the 1 Ms exposure (see Brandt *et al.* 2001b).†

Six extended X-ray sources have also been detected in the CDF-N (Bauer *et al.* 2002). Their X-ray spectral properties, angular sizes, and likely luminosities ($\approx 10^{42}$ erg s^{-1}) are generally consistent with those found for nearby groups of galaxies. Two extended X-ray sources of note are (1) a group in the HDF-N associated with the $z = 1.013$ FR I radio galaxy VLA J123644.3+621133, and (2) a likely poor-to-moderate cluster at $z \gtrsim 0.7$ that is coincident with an overdensity of Very Red Objects (VROs; $I - K \geq 4$), optically faint ($I \geq 24$) radio sources,

† http://www.astro.psu.edu/users/niel/hdf/hdf-chandra.html

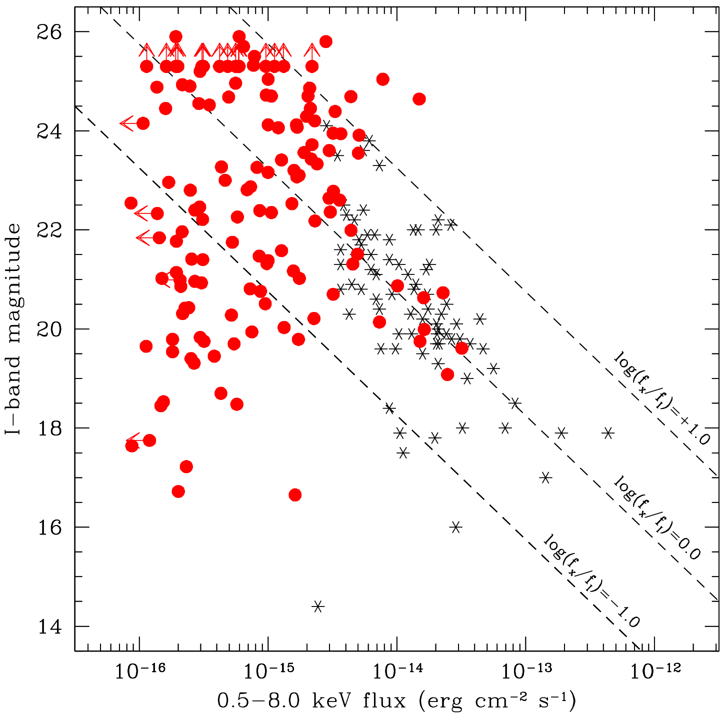

Figure 3. I-band magnitude versus full-band X-ray flux for X-ray sources from an $8.4' \times 8.4'$ region of the CDF-N field centred on the HDF-N (solid dots; Alexander *et al.* 2001) and the *ROSAT* ultra deep survey of the Lockman Hole (stars; converted to 0.5–8 keV; Lehmann *et al.* 2001). The dashed diagonal lines indicate constant X-ray to I-band flux ratios; luminous AGN typically have $\log(f_X/f_I)$ in the range from -1 to $+1$. Note the wide spread of I-band magnitudes for the faintest X-ray sources.

and optically faint X-ray sources. The surface density of extended X-ray sources is 167^{+97}_{-67} deg^{-2} at a limiting soft-band flux of $\approx 3 \times 10^{-16}$ erg cm^{-2} s^{-1}. No evolution in the X-ray luminosity function of clusters is needed to explain this value.

Fig. 3 shows the I-band magnitudes of the X-ray point sources near the centre of the CDF-N field. There is a wide spread of I-band magnitudes at faint X-ray fluxes, corresponding to a range of source types. The faint X-ray sources with $I \approx$ 15–22 counterparts are normal galaxies, starburst galaxies, low-luminosity AGN, and stars. The faint X-ray sources with $I \gtrsim 22$ counterparts appear to be mostly luminous AGN; these often show evidence for X-ray absorption via large hardness ratios.

Optical spectra are presently available for ≈ 120 CDF-N objects. The majority of the sources with spectroscopic redshifts lie at $z \lesssim 1.3$ (see Fig. 4). This result is at least partially due to a selection effect: as implied by Fig. 4, the X-ray sources at $z \gtrsim 1.3$ will frequently be too optically faint for spectroscopy (with $I \gtrsim 24$). These sources are discussed further in §2d. Even after making plausible corrections for selection effects, however, it appears likely that more X-ray power originates from

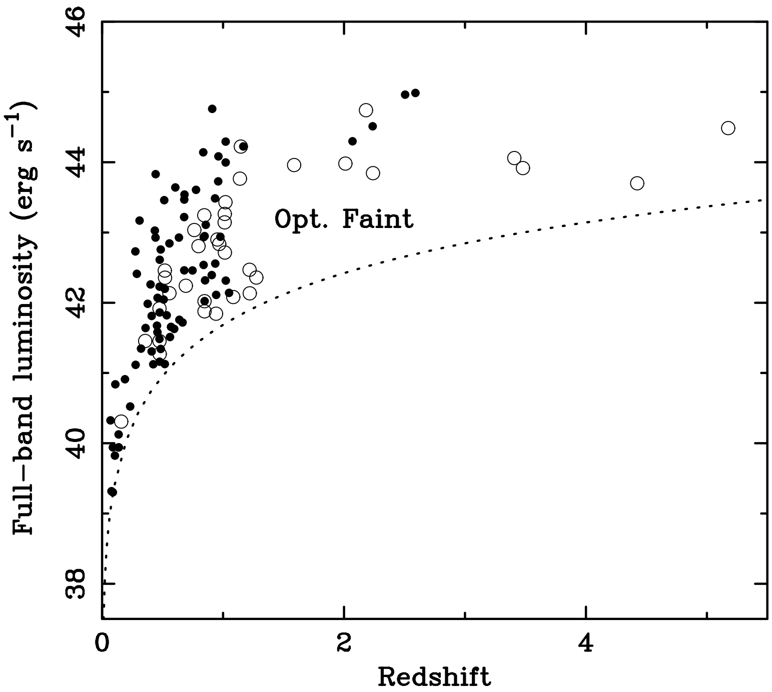

Figure 4. Full-band X-ray luminosity versus redshift for X-ray sources with optical spectra. Solid dots are sources with $I < 21.5$, and open circles are sources with $I > 21.5$. The dotted curve represents the X-ray detection limit. Note that most of the sources at $z \approx 1$–1.3 have $I > 21.5$. Similar sources at $z \gtrsim 1.3$ (in the region marked "Opt. Faint") will frequently have $I \gtrsim 24$ and thus be too optically faint for spectroscopy (see also Fig. 8b).

$z \lesssim 1.3$ than predicted by some X-ray background synthesis models; these models will require revision.

(*b*) *Results for the Hubble Deep Field-North*

Fig. 5 shows the 27 HDF-N X-ray point sources detected thus far (Hornschemeier *et al.* 2000; Brandt *et al.* 2001a; W.N. Brandt *et al.*, in preparation); 16 are found with a false-source probability threshold of 1×10^{-7} while the other 11 are found with lower significance but align spatially with optical galaxies (see §2a). As expected from Figs. 3 and 4, most sources are at $z < 1.5$, and their optical counterparts have a wide range of brightness. In at least one HDF-N object (CXO-HDFN J123641.7+621131 at $z = 0.089$) the X-ray source is offset from the nucleus; the X-ray emission may arise from a starburst region in the host galaxy as it is coincident with a bright, blue "knot."

We have been able to find likely optical or near-infrared counterparts for all of the X-ray sources in the HDF-N; this contrasts with the case in the radio where some truly "blank-field" sources have been found (e.g., Richards *et al.* 1999). We find a good correspondence between our brighter X-ray sources and micro-Jy radio (1.4 GHz and 8.5 GHz) sources, but this trend does not continue for our faintest X-ray sources. For instance, 10 of the 16 brightest *Chandra* sources have radio matches, but only 12 of the 27 total *Chandra* sources have radio matches. The properties

Figure 5. *Chandra* sources detected in the HDF-N circled on the *HST* optical image. Solid circles indicate sources detected with a false-positive probability threshold of 1×10^{-7}, and broken circles indicate sources found at lower significance levels that are spatially correlated with optical galaxies (see §2a). The numbers are source redshifts; redshifts followed by a "p" are photometric rather than spectroscopic. The extended source in the HDF-N (see §2a) is located near the $z = 1.013$ FR I radio galaxy at the bottom of the image.

of the X-ray/radio sources suggest a broad range of emission mechanisms (e.g., Richards *et al.* 1998; Brandt *et al.* 2001a). We also find a good correspondence between *Chandra* and *ISO* (6.7 μm and 15 μm; Aussel *et al.* 1999) sources in the HDF-N. Ten of the 16 brightest *Chandra* sources have *ISO* matches, and 14 of the 27 total *Chandra* sources have *ISO* matches. This good X-ray/IR correspondence bodes well for future IR follow-up of X-ray sources with *SIRTF* (see §3b). In this field with both exceptionally sensitive X-ray and IR coverage, we find a broad range of X-ray/IR source types including starburst galaxies, obscured AGN, and normal elliptical galaxies. In the majority of the sources, the IR emission appears to be from dust re-emission of primary X-ray and ultraviolet radiation.

(*c*) *X-ray Connections with Infrared, Radio and Submillimeter Sources*

More detailed studies of the X-ray/IR sources in the CDF-N have recently been completed by Alexander *et al.* (2002b) and Fadda *et al.* (2002). These use the 21.5 arcmin^2 region with uniform *ISO* coverage at 15 μm rather than just the HDF-N (5.3 arcmin^2). Only $\approx 20\%$ of the X-ray/IR sources are likely AGN. The

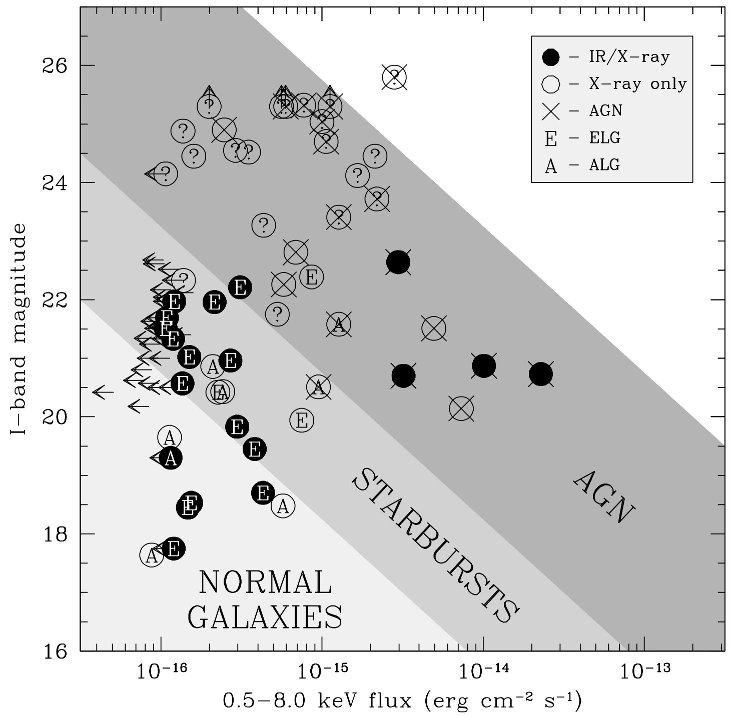

Figure 6. I-band magnitude versus full-band X-ray flux for sources with both deep *Chandra* and *ISO* coverage. The filled circles are the X-ray/IR matched sources, and the open circles are X-ray sources without IR counterparts. Characters inside the circles indicate different source types: "E" indicates emission-line galaxies, "A" indicates absorption-line galaxies, "?" indicates sources that do not have spectroscopic classifications, and overlaid crosses indicate AGN-dominated sources. IR sources without detected X-ray emission are plotted only as upper-limit arrows. The shaded regions delineate the approximate range of X-ray-to-optical flux ratio for AGN-dominated sources, starburst galaxies, and normal galaxies. Adapted from Alexander *et al.* (2002b).

majority rather appear to be $z \approx 0.4$–1.3 starburst galaxies and $z < 0.2$ normal galaxies (see Fig. 6). A notable finding is that up to 100% of the X-ray detected emission-line galaxies (see Cohen *et al.* 2000 for the optical spectral classification) have 15 μm counterparts (Alexander *et al.* 2002b); the majority of these are luminous IR starburst galaxies representative of the population making the bulk of the IR background. The X-ray/radio matched galaxies trace the same star-forming population as the X-ray/IR sources with nearly 100% of the matched galaxies in common (F.E. Bauer *et al.*, in preparation). In addition, the X-ray/radio matches appear to trace a population of optically faint AGN.

Barger *et al.* (2001b) have shown that the ensemble of CDF-N X-ray sources contribute about 15% of the extragalactic submillimeter background light at 850 μm, with the strongest submillimeter emission being seen from optically faint X-ray sources that are also detected at 1.4 GHz. At the current CDF-N flux limit, $\approx 20\%$ of the submillimeter sources have X-ray counterparts.

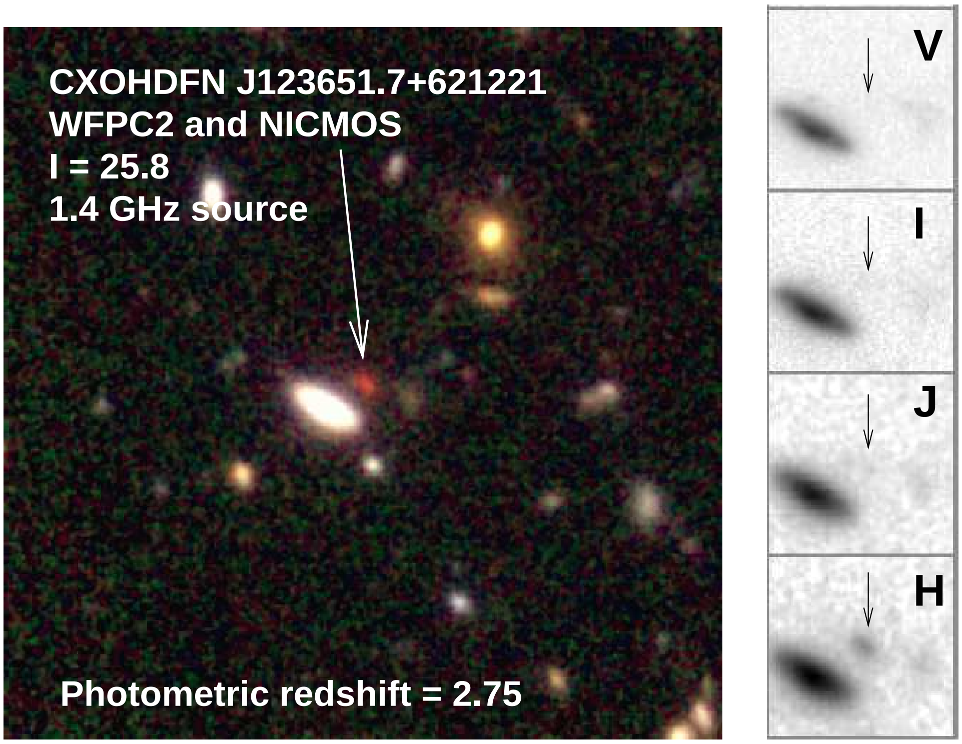

Figure 7. CXOHDFN J123651.7+621221, an example of an optically faint X-ray source lying in the HDF-N. This $I = 25.8$ source has a photometric redshift of $z = 2.75$ (e.g., Alexander *et al.* 2001) and is remarkably red (compare the V-band to H-band images shown). It is the hardest as well as the second X-ray brightest source found in the HDF-N. The X-ray luminosity ($\approx 3 \times 10^{44}$ erg s^{-1}) and hard spectral shape indicate this source is a luminous, obscured AGN. It was previously noted as an optically faint micro-Jy radio source (e.g., Richards *et al.* 1999) and thought to be a dusty starburst galaxy (e.g., Muxlow *et al.* 1999). The NICMOS images were kindly provided by M. Dickinson (see Dickinson *et al.* 2000).

(*d*) *Optically Faint and High-Redshift X-ray Sources*

As mentioned in §2a, a significant fraction of the CDF-N X-ray sources are too optically faint for easy spectroscopic follow-up studies. One notable example from the HDF-N is shown in Fig. 7. Alexander *et al.* (2001) present a detailed study of the 47 optically faint X-ray sources (defined as having $I \geq 24$) in an $8.4' \times 8.4'$ region centred on the HDF-N. The number of optically faint X-ray sources increases at faint X-ray fluxes. However, the fraction of optically faint sources within the X-ray source population stays roughly constant at $\approx 35\%$ for full-band fluxes from 10^{-16}–10^{-14} erg cm^{-2} s^{-1} due to the emergence of a population of optically bright sources (see §2a and Fig. 3). Many of the optically faint X-ray sources have red optical-to-near-IR colours, and a significant fraction are classified as VROs (see also Alexander *et al.* 2002a for a detailed X-ray study of CDF-N VROs). They also have harder X-ray spectra on average than the sources with $I < 24$ (see Fig. 8a). Roughly half of the optically faint sources with enough X-ray counts to allow an

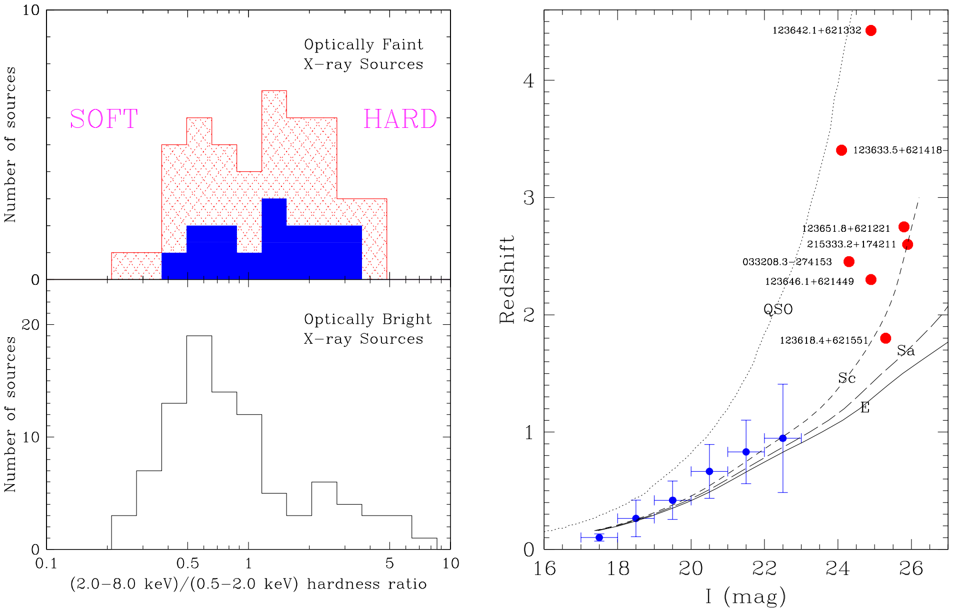

Figure 8. (a) X-ray hardness ratio distributions for optically faint ($I \geq 24$) and optically bright source samples. While both samples have a wide spread in hardness ratio, the optically faint sources are harder on average. The solid shading in the upper panel shows the subset of optically faint sources without I-band detections (corresponding to $I > 25.3$). (b) Redshift versus I-band magnitude for X-ray sources. The small solid dots with error bars show the average spectroscopic redshifts of the $I < 23$ X-ray sources as a function of I-band magnitude. The large solid dots show individual optically faint X-ray sources with spectroscopic, photometric or millimetric redshifts. The labelled curves in the diagram show tracks for an $M_{\rm I} = -23$ E galaxy, Sa galaxy, Sc galaxy, and QSO. Note that the $I < 23$ X-ray sources follow the galaxy tracks fairly well; their optical emission appears to be dominated by that from the host galaxy. If the same holds for the optically faint X-ray sources, extrapolation along the curves indicates the majority should lie at $z \approx 1$–3. This is indeed consistent with that found for the few optically faint sources with redshift determinations. Adapted from Alexander *et al.* (2001).

effective search for X-ray variability show it, and the redshifts of the majority of the optically faint X-ray sources are estimated to be $z \approx 1$–3 (see Fig. 8b). All of these facts support an interpretation where most of the optically faint X-ray sources are luminous, obscured AGN (e.g., Seyfert 2 galaxies and type 2 quasars) at intermediate redshifts.

A minority of the optically faint X-ray sources, however, may be AGN at high-to-extreme redshifts ($z \approx 4$–10). One notable example is CXOHDFN J123642.0+621331 (Brandt *et al.* 2001a; $I = 25.3$) which lies just outside the HDF-N and is a micro-Jy radio source at a likely redshift of $z = 4.424$ (Waddington *et al.* 1999). With an X-ray luminosity of $\approx 5 \times 10^{43}$ erg s^{-1}, this is by far the lowest luminosity X-ray source known at $z > 4$. Its detection directly demonstrates that *Chandra* is achieving the sensitivity needed to study Seyfert-luminosity AGN at high redshift.

A large population of Seyfert-luminosity AGN at $z \approx 4$–10 has been postulated

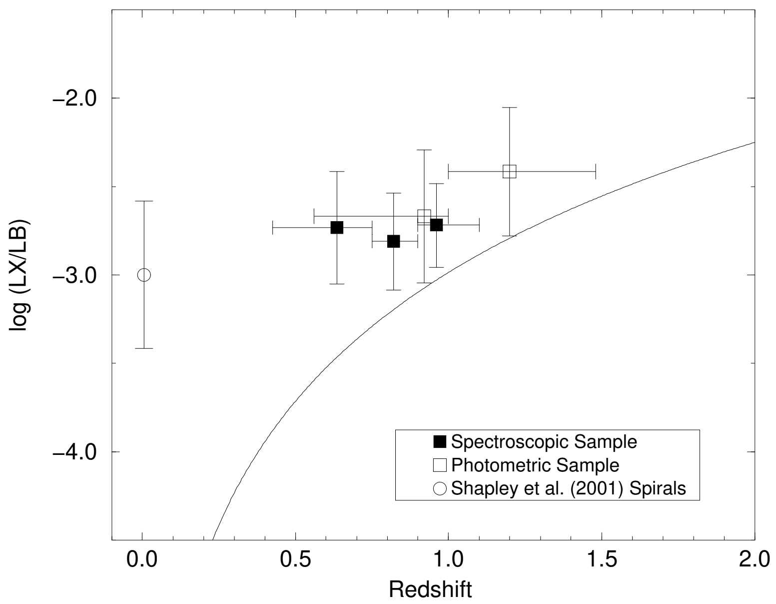

Figure 9. $\log(L_{\rm X}/L_{\rm B})$ as a function of redshift for stacked samples of $\approx L_{\rm B}^{*}$ spiral galaxies ($L_{\rm X}$ is for 0.5–2 keV); samples with both spectroscopically and photometrically derived redshifts are shown. The solid curve indicates the 2σ X-ray sensitivity limit normalized by $L_{\rm B}^{*}$. The data point at $z \approx 0$ is derived from Shapley *et al.* (2001). Adapted from Hornschemeier *et al.* (2002).

by Haiman & Loeb (1999). These objects would represent the first massive black holes to form in the Universe. At $z \gtrsim 6.5$ an AGN should appear not only optically faint but optically blank; the Lyman α forest and Gunn-Peterson trough will absorb essentially all flux through the I band. Thus, an upper limit on the space density of extreme redshift AGN can be set simply by counting the number of X-ray sources that lack any optical counterpart.† Unfortunately, however, confusion between truly optically blank sources at extreme redshift and very optically faint sources at moderate redshift (e.g., objects like that in Fig. 7) occurs without exceptionally deep optical imaging. At present, the CDF-N data suggest that there is $\lesssim 1$ AGN detected at $z \gtrsim 6.5$ per ≈ 12 arcmin^2 (Alexander *et al.*. 2001). This limit should soon be tightened substantially via the GOODS project (see §3b).

The highest redshift AGN discovered in CDF-N follow-up studies has $z = 5.18$ (A.J. Barger *et al.*, in preparation). This is the highest redshift X-ray selected AGN, and it has relatively narrow emission lines. This source is not optically faint ($I = 22.7$) and has an X-ray luminosity of $\approx 3 \times 10^{44}$ erg s^{-1}; it could have been detected by *Chandra* out to $z \approx 10$.

† Of course, this method requires the plausible assumption that extreme redshift AGN be X-ray luminous. The best available data suggest that this should be the case (e.g., Vignali *et al.* 2001; Brandt *et al.* 2002). Note also that at $z \approx 10$ *Chandra* provides rest-frame sensitivity up to ≈ 90 keV; such high-energy X-rays can penetrate a substantial amount of obscuration.

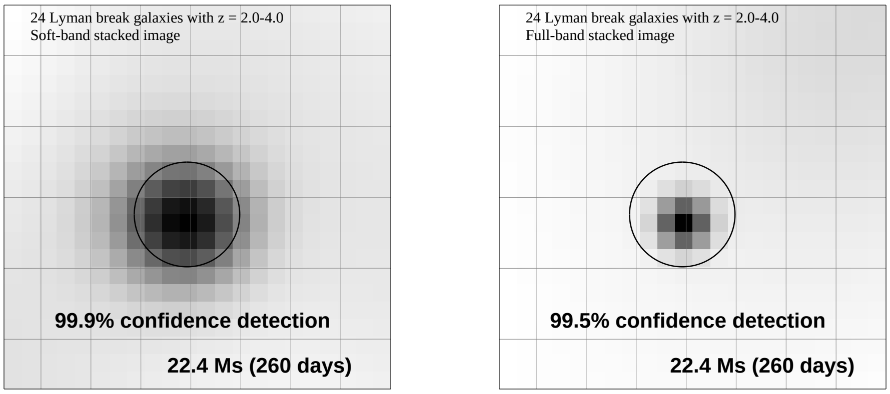

Figure 10. Stacked soft-band and full-band *Chandra* images of 24 HDF-N Lyman break galaxies at $z = 2$–4. The black circles are centred on the stacking position and have radii of $1.5''$. The effective exposure time for the average Lyman break galaxy is 22.4 Ms (260 days). Both bands give highly significant detections, as assessed with a Monte Carlo technique. Adapted from Brandt *et al.* (2001c).

(*e*) *Stacking Studies of Galaxies at Cosmologically Interesting Distances*

At the fainter X-ray fluxes of the CDF-N, a significant number of "normal" galaxies are detected at $z \lesssim 0.3$ where the observed emission appears to originate from X-ray binaries, ultraluminous X-ray sources, supernova remnants, and perhaps low-luminosity AGN (e.g., Hornschemeier *et al.* 2001; A.E. Hornschemeier *et al.*, in preparation). For example, in the HDF-N *Chandra* has detected all optically luminous galaxies out to $z = 0.15$ (Brandt *et al.* 2001a).

X-ray studies of normal galaxies at cosmological distances are of importance since normal galaxies are expected to be the most numerous extragalactic X-ray sources at the faintest X-ray fluxes; in Fig. 5 there are ~ 3000 galaxies but only 27 X-ray sources, so "there's plenty of room at the bottom" (cf. Feynman 1960). Normal galaxies are expected to dominate the number counts at soft-band fluxes of $\approx 5 \times 10^{-18}$ erg cm^{-2} s^{-1} (e.g., Ptak *et al.* 2001; Hornschemeier *et al.* 2002; Miyaji & Griffiths 2002), and they should be one of the main source types detected by missions such as *XEUS* and *Generation-X*. Furthermore, the X-ray properties of galaxies might well have changed in response to the substantial change in the cosmic star formation rate over the history of the Universe; changes in the star formation rate should affect the production of X-ray binaries and supernovae (e.g., Ghosh & White 2001).

Most normal galaxies at $z \gtrsim 0.3$ cannot be individually detected in the current CDF-N data, but their average properties can be probed using stacking techniques where the X-ray emission from many individually undetected galaxies is added together. Using stacking techniques, Hornschemeier *et al.* (2002) have measured the average X-ray luminosities of $\approx L_{\rm B}^*$ spiral galaxies out to $z = 1.2$, corresponding to a look-back time of ≈ 9.0 Gyr. These measurements allow the first reliable predictions of the number of normal galaxies that should be seen in deeper X-ray exposures; typical observed soft-band fluxes are $\approx (3$–$7)\times 10^{-18}$ erg cm^{-2} s^{-1}.

There is evidence for a factor of 2–3 increase in X-ray luminosity (per unit B-band luminosity) with redshift (see Fig. 9), although this is weaker than some theoretical models have predicted.

At higher redshifts ($z = 2$–4), X-ray stacking analyses have allowed an average detection of the Lyman break galaxies in the HDF-N (see Fig. 10; Brandt *et al.* 2001c). In the rest-frame ultraviolet and optical bands these galaxies share many of the properties of local starburst galaxies and have estimated star formation rates of $\approx$ 20–50 $M_{\odot}$ yr^{-1}. We find their average X-ray luminosity ($\approx 3 \times 10^{41}$ erg s^{-1} in the rest-frame 2–8 keV band) to be similar to those of the most luminous local starburst galaxies (these have star formation rates comparable to those estimated for the Lyman break galaxies). For Lyman break galaxies, the observed ratio of X-ray to B-band luminosity is somewhat, but not greatly, higher than that seen from local starburst galaxies.

3. The Future

(*a*) *Additional X-ray Coverage*

The current CDF-N survey is far from the limit of *Chandra*'s capability. The full-band detector background is so low that, with appropriate grade screening, *Chandra* will not fully enter the background-limited regime near the aim point for exposure times of $\lesssim$ 5 Ms. In the soft band the situation is even better due to the lower background, and *Chandra* should remain photon limited to $\approx$ 10 Ms. At present, *Chandra* observation time is allocated to extend the survey to 2 Ms, and additional observations will be proposed.

Fig. 11 shows that with sufficient exposure (5–10 Ms), *Chandra* surveys can reach depths comparable to those discussed for missions such as *XEUS*. They would thereby bolster the science cases for missions such as *XEUS* and *Generation-X*, providing key information on the existence and nature of the sources to be targeted by these missions. Important targets would include the first massive black holes at high redshift as well as normal and starburst galaxies at intermediate redshift. Detailed spectral, temporal, and spatial constraints would be obtained for all the sources currently detected. Furthermore, Fig. 11 shows that *Chandra* positions are likely to be the best available for $\gtrsim$ 15–20 years; these will be essential for the reliable identification of optically faint sources at high redshift.

(*b*) *Observations at Other Wavelengths*

Multiwavelength follow-up studies of the CDF-N sources continue, and a catalog presenting the current optical photometric and spectroscopic results will be completed shortly (A.J. Barger *et al.*, in preparation). The Great Observatories Origins Deep Survey (GOODS) project will soon obtain deep, public *HST* Advanced Camera for Surveys and *SIRTF* coverage over the deepest $\approx$ 1/3 of the CDF-N (see Fig. 1).† These projects, along with others already completed and in progress, will provide a panchromatic data set with the sensitivity and angular resolution needed to complement fully the CDF-N.

† http://www.stsci.edu/science/goods/

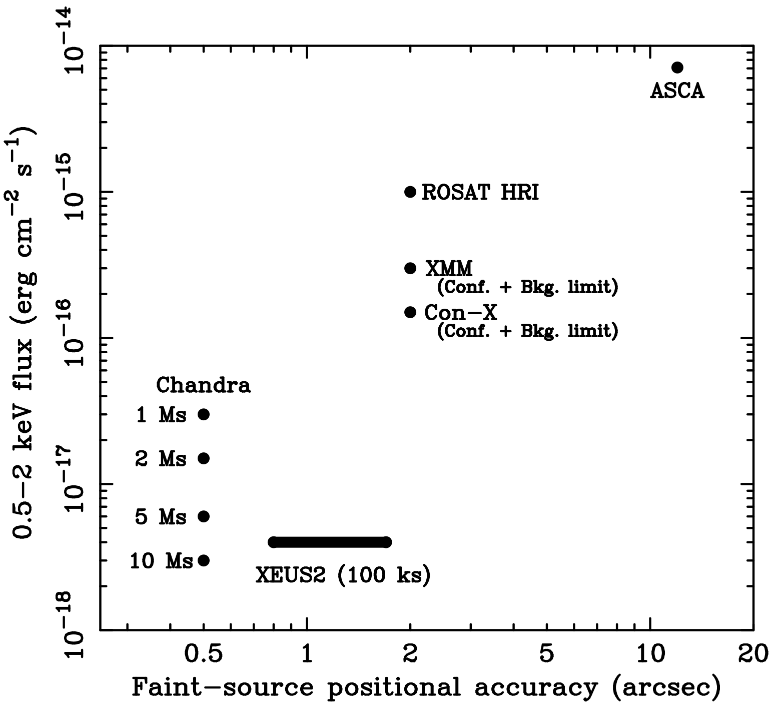

Figure 11. Flux limit versus faint-source positional accuracy for some past, present, and future X-ray missions. Note that the locations in the diagram for future missions should be taken as approximate, and that *Constellation-X* is focused on high-throughput spectroscopy rather than deep surveys. Both *XMM-Newton* and *Constellation-X* are background limited and suffer from source confusion at approximately the positions shown. With sufficient exposure, *Chandra* can achieve sensitivities comparable to those discussed for future missions such as *XEUS*. Furthermore, *Chandra* positions are likely to be the best available for $\gtrsim$ 15–20 years.

We thank all the members of the CDF-N team. This work would not have been possible without the efforts of the entire *Chandra* and ACIS teams. We gratefully acknowledge the financial support of NASA grant NAS 8-38252 (Gordon P. Garmire, PI), NSF CAREER award AST-9983783 (WNB, DMA, FEB), and NASA GSRP grant NGT 5-50247 and the Pennsylvania Space Grant Consortium (AEH).

References

Alexander, D.M., Brandt, W.N., Hornschemeier, A.E., Garmire, G.P., Schneider, D.P., Bauer, F.E. & Griffiths, R.E. 2001 The Chandra Deep Field-North survey. VI. The nature of the optically faint X-ray source population. *The Astronomical Journal*, **122**, 2156–2176.

Alexander, D.M., Vignali, C., Bauer, F.E., Brandt, W.N., Hornschemeier, A.E., Garmire, G.P. & Schneider, D.P. 2002a The Chandra Deep Field-North survey. X. X-ray emission from Very Red Objects. *The Astronomical Journal*, in press (astro-ph/0111397).

Alexander, D.M., Aussel, H., Bauer, F.E., Brandt, W.N., Hornschemeier, A.E., Vignali, C., Garmire, G.P. & Schneider, D.P. 2002b The Chandra Deep Field-North survey. XI.

X-ray emission from luminous infrared starburst galaxies. *The Astrophysical Journal*, submitted.

Aussel, H., Cesarsky, C.J., Elbaz, D. & Starck, J.L. 1999 ISOCAM observations of the Hubble Deep Field reduced with the PRETI method. *Astronomy & Astrophysics*, **342**, 313–336.

Barger, A.J., Cowie, L.L., Mushotzky, R.F. & Richards, E.A. 2001a The nature of the hard X-ray background sources: Optical, near-infrared, submillimeter, and radio properties. *The Astronomical Journal*, **121**, 662–682.

Barger, A.J., Cowie, L.L., Steffen, A.T., Hornschemeier, A.E., Brandt, W.N., & Garmire, G.P., 2001b Submillimeter properties of the 1 Ms Chandra Deep Field-North X-ray sample. *The Astrophysical Journal*, **560**, L23–L28.

Bauer, F.E., *et al.* 2002 The Chandra Deep Field-North survey. IX. Extended X-ray sources. *The Astronomical Journal*, in press (astro-ph/0112002).

Brandt, W.N., *et al.* 2000 Observations of faint, hard-band X-ray sources in the field of CRSS J0030.5+2618 with the Chandra X-ray Observatory and the Hobby-Eberly Telescope. *The Astronomical Journal*, **119**, 2349–2359.

Brandt, W.N., *et al.* 2001a The Chandra deep survey of the Hubble Deep Field-North area. IV. An ultradeep image of the Hubble Deep Field-North. *The Astronomical Journal*, **122**, 1–20.

Brandt, W.N., *et al.* 2001b The Chandra Deep Field-North survey. V. 1 Ms source catalogs. *The Astronomical Journal*, **122**, 2810–2832.

Brandt, W.N., Hornschemeier, A.E., Schneider, D.P., Alexander, D.M., Bauer, F.E., Garmire, G.P. & Vignali, C. 2001c The Chandra Deep Field-North survey. VII. X-ray emission from Lyman break galaxies. *The Astrophysical Journal*, **558**, L5–L9.

Brandt, W.N., *et al.* 2002 Exploratory Chandra observations of the three highest redshift quasars. *The Astrophysical Journal*, submitted (astro-ph/0202235).

Cohen, J.G., Hogg, D.W., Blandford, R., Cowie, L.L., Hu, E., Songaila, A., Shopbell, P., & Richberg, K. 2000 Caltech faint galaxy redshift survey. X. A redshift survey in the region of the Hubble Deep Field-North. *The Astrophysical Journal*, **538**, 29–52.

Cowie, L.L., Garmire, G.P., Bautz, M.W., Barger, A.J., Brandt, W.N. & Hornschemeier, A.E. 2002 2–8 keV X-ray number counts determined from Chandra blank field observations. *The Astrophysical Journal*, 566, L5–L8.

Dickinson, M., *et al.* 2000 The unusual infrared object HDF-N J123656.3+621322. *The Astrophysical Journal*, **531**, 624–634.

Ebeling, H., White, D.A. & Rangarajan, F.V.N. 2002 ASMOOTH: A simple and efficient algorithm for adaptive kernel smoothing of two-dimensional imaging data. *Monthly Notices of the Royal Astronomical Society*, submitted.

Fabian, A.C. & Barcons, X. 1992 The origin of the X-ray background. *Annual Reviews of Astronomy and Astrophysics*, **30**, 429–456.

Fadda, D., Flores, H., Hasinger, G., Franceschini, A., Altieri, B., Cesarsky, C.J., Elbaz, D. & Ferrando, Ph. 2002 The AGN contribution to mid-infrared surveys: X-ray counterparts of the mid-infrared sources in the Lockman Hole and HDF. *Astronomy & Astrophysics*, in press (astro-ph/0111412).

Ferguson, H.C., Dickinson, M. & Williams, R. 2000 The Hubble Deep Fields. *Annual Reviews of Astronomy & Astrophysics*, **38**, 667–715.

Feynman, R.P. 1960 There's Plenty of Room at the Bottom. *Engineering and Science*, February 1960 issue, California Institute of Technology, USA.

Freeman, P.E., Kashyap, V., Rosner, R. & Lamb, D.Q. 2002 A wavelet-based algorithm for the spatial analysis of Poisson data. *The Astrophysical Journal Supplements*, 138, 185–218.

Ghosh, P. & White, N.E. 2001 X-ray probes of cosmic star-formation history. *The Astrophysical Journal*, **559**, L97–L100.

Giacconi, R., Gursky, H., Paolini, F.R. & Rossi, B.B. 1962 Evidence for X-rays from sources outside the solar system. *Physical Review Letters*, **9**, 439–443.

Giacconi, R., *et al.* 2001 First results from the X-ray and optical survey of the Chandra Deep Field South. *The Astrophysical Journal*, **551**, 624–634.

Giacconi, R., *et al.* 2002 Chandra Deep Field South: The 1 Ms source catalog. *The Astrophysical Journal Supplements*, in press (astro-ph/0110452).

Haiman, Z. & Loeb, A. 1999 X-ray emission from the first quasars. *The Astrophysical Journal*, **521**, L9–L12.

Hasinger, G., Burg, R., Giacconi, R., Schmidt, M., Trümper, J. & Zamorani, G. 1998 The ROSAT deep survey: I. X-ray sources in the Lockman field. *Astronomy & Astrophysics*, **329**, 482–494.

Hasinger, G. 2000 X-ray surveys of the obscured Universe. In *ISO Surveys of a Dusty Universe* (ed. D. Lemke, M. Stickel & K. Wilke). Springer Lecture Notes in Physics, no. 548, 423–431.

Hasinger, G., *et al.* 2001 XMM-Newton observations of the Lockman Hole. I. The X-ray data. *Astronomy & Astrophysics*, **365**, L45–L50.

Hornschemeier, A.E., *et al.* 2000 X-ray sources in the Hubble Deep Field-North detected by Chandra. *The Astrophysical Journal*, **541**, 49–53.

Hornschemeier, A.E., *et al.* 2001 The Chandra deep survey of the Hubble Deep Field-North area. II. Results from the Caltech Faint Field Galaxy Redshift Survey area. *The Astrophysical Journal*, **554**, 742–777.

Hornschemeier, A.E., Brandt, W.N., Alexander, D.M., Bauer, F.E., Garmire, G.P., Schneider, D.P., Bautz, M.W. & Chartas, G. 2002 The Chandra Deep Field-North survey. VIII. X-ray constraints on spiral galaxies from $0.4 < z < 1.5$. *The Astrophysical Journal*, in press (astro-ph/0110094).

Jansen, F., *et al.* 2001 XMM-Newton observatory: I. The spacecraft and operations. *Astronomy & Astrophysics*, **365**, L1–L6.

Lehmann, I., *et al.* 2001 The ROSAT deep survey. VI. X-ray sources and optical identifications of the ultra deep survey. *Astronomy & Astrophysics*, **371**, 833–857.

Miyaji, T. & Griffiths, R.E. 2002 Faint-source counts from off-source fluctuation analysis on Chandra observations of the Hubble Deep Field-North. *The Astrophysical Journal*, **564**, L5–L8.

Mushotzky, R.F., Cowie, L.L., Barger, A.J. & Arnaud, K.A. 2000 Resolving the extragalactic hard X-ray background. *Nature*, **404**, 459–464.

Muxlow, T.W.B., Wilkinson, P.N., Richards, A.M.S., Kellermann, K.I., Richards, E.A. & Garrett, M.A. 1999 High-resolution imaging of the Hubble Deep and flanking fields. *New Astronomy Reviews*, **43**, 623–627.

Ptak, A., Griffiths, R., White, N. & Ghosh, P. 2001 The consequences of the cosmic star-formation rate: X-ray number counts. *The Astrophysical Journal*, **559**, L91–L95.

Richards, E.A., Kellermann, K.I., Fomalont, E.B., Windhorst, R.A. & Partridge, R.B. 1998 Radio emission from galaxies in the Hubble Deep Field. *The Astronomical Journal*, AJ, **116**, 1039–1054.

Richards, E.A., Fomalont, E.B., Kellermann, K.I., Windhorst, R.A., Partridge, R.B., Cowie, L.L. & Barger, A.J. 1999 Optically faint microjansky radio sources. *The Astrophysical Journal*, **526**, L73–L76.

Rosati, P., *et al.* 2002 The Chandra Deep Field South: The 1 million second exposure. *The Astrophysical Journal*, in press (astro-ph/0110452).

Shapley, A., Fabbiano, G. & Eskridge, P.B. 2001 A multivariate statistical analysis of spiral galaxy luminosities. I. Data and results. *The Astrophysical Journal Supplements*, **137**, 139–199.

Vignali, C., Brandt, W.N., Fan, X., Gunn, J.E., Kaspi, S., Schneider, D.P. & Strauss, M.A. 2001 Exploratory Chandra observations of the highest-redshift quasars: X-rays from the dawn of the modern Universe. *The Astronomical Journal*, **122**, 2143–2155.

Waddington, I., Windhorst, R.A., Cohen, S.H., Partridge, R.B., Spinrad, H. & Stern, D. 1999 NICMOS imaging of the dusty microJanky radio source VLA J123642+621331 at $z = 4.424$. *The Astrophysical Journal*, **526**, L77–L80.

Weisskopf, M.C., Tananbaum, H.D., Van Speybroeck, L.P. & O'Dell, S.L. 2000 Chandra X-ray Observatory (CXO): overview. *Proc. SPIE*, **4012**, 2–16.